

^{133}Cs NMR investigation of 2D frustrated Heisenberg antiferromagnet, Cs_2CuCl_4

M. -A. Vachon, W. Kundhikanjana, A. Straub, and V. F. Mitrović

Department of Physics, Brown University, Providence, RI 02912, U.S.A.

A. P. Reyes and P. Kuhns

National High Magnetic Field Laboratory, Tallahassee, FL 32310, U.S.A.

R. Coldea

Department of Physics, University of Bristol, Bristol BS8 1TL, UK

Z. Tylczynski

Institute of Physics, Adam Mickiewicz University, Umultowska 85, 61-614 Poznan, Poland

Abstract. We report ^{133}Cs nuclear magnetic resonance (NMR) measurements on the 2D frustrated Heisenberg antiferromagnet Cs_2CuCl_4 down to 2 K and up to 15 T. We show that ^{133}Cs NMR is a good probe of the magnetic degrees of freedom in this material. Cu spin degrees of freedom are sensed through a strong anisotropic hyperfine coupling. The spin excitation gap opens above the critical saturation field. The gap value was determined from the activation energy of the nuclear spin-lattice relaxation rate in a magnetic field applied parallel to the Cu chains (\hat{b} axis). The values of the g -factor and the saturation field are consistent with the neutron-scattering and magnetization results. The measurements of the spin-spin relaxation time are exploited to show that no structural changes occur down to the lowest temperatures investigated.

PACS numbers: 71.35.Ji, 75.30.Cr, 75.40.Cx

1. Introduction

Two dimensional quantum antiferromagnets on geometrically-frustrated lattices have been theoretically proposed to show strongly correlated physics and possibly spin liquid states with no long-range magnetic order and fractional spin excitations (for a review see for example Ref. [1]). In this respect the quasi-two-dimensional insulating spin-1/2 antiferromagnet Cs_2CuCl_4 with spins on an anisotropic triangular lattice has recently attracted much experimental [2, 3] and theoretical interest [4, 5, 6, 7, 8, 9, 10, 11]. Neutron scattering measurements have revealed several unusual features in the spin dynamics that have been interpreted in terms of proximity to a spin liquid state [4, 5, 6, 7, 8, 9]. The question of the existence of a gap is central to the issue of the spin-liquid classification [1]. NMR as a low-energy probe of the spin degrees of freedom could potentially provide direct information about the low-energy spin dynamics and the presence of a small spin gap in the field induced phases.

Here we report on extensive ^{133}Cs NMR measurements in single crystals of Cs_2CuCl_4 in fields up to 15 T, applied parallel and perpendicular to the magnetic planes, and at temperatures down to 2 K. Both static and dynamic measurements reveal that ^{133}Cs NMR is a sensitive probe of the magnetism of Cu ions. The strength of the Cs hyperfine coupling is deduced. From the activation energy of the nuclear spin-lattice relaxation rate we confirm that a Zeeman gap opens at high fields above the ferromagnetic saturation field, H_{sat} . The gap value is consistent with the gap determined by neutron scattering measurements. Exploiting the spin-spin relaxation time measurements, we show that no structural changes occur down to the lowest temperatures investigated.

The rest of the paper is organized as follows. The crystal structure and magnetic properties of Cs_2CuCl_4 are described in Sec. 2. In Sec. 3, we present measurements of the spin shift and use these to extract hyperfine coupling constants. In Sec. 4, measurements of the nuclear spin-lattice relaxation rate T_1^{-1} are used to determine spin gap values. In addition, we discuss a special technique that was employed to measure the rate. Finally, the spin-spin relaxation rates are discussed in Sec. 5. These measurements are used to deduce quadrupole coupling parameters at low temperatures.

2. Crystal Structure, Magnetism, and Experimental Details

The crystal structure of Cs_2CuCl_4 is orthorhombic with space group $Pnma$ and lattice parameters $a = 9.65 \text{ \AA}$, $b = 7.48 \text{ \AA}$, and $c = 12.35 \text{ \AA}$ at $T = 0.3 \text{ K}$ [12]. As displayed in Fig. 1(a), each unit cell consists of four CuCl_4^{2-} tetrahedra and eight Cs atoms. The tetrahedra form a linear chain in the \hat{b} direction with two Cl between each Cu. The chains are stacked together along the \hat{c} direction, displaced by $b/2$ with respect to each other. The planes are stacked together along the \hat{a} direction. In this structure there are two inequivalent cesium nuclear sites, labeled as Cs(A) and Cs(B). The Cs(A) atoms, surrounded by eleven Cl at a mean distance of 3.79 \AA are located in the center of the Cu triangles close to the plane. The Cs(B) atoms, surrounded by nine Cl at a mean distance

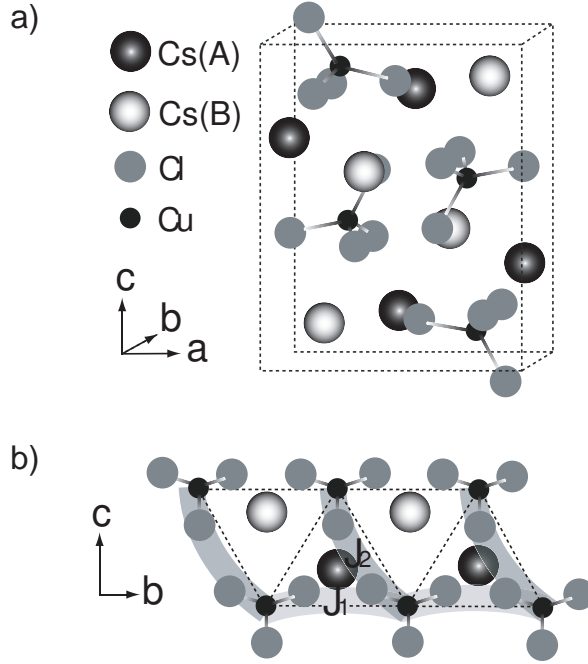


Figure 1. (a) Unit cell of Cs_2CuCl_4 with the Cu^{2+} ions displayed as small black spheres in the center of the tetrahedra formed by the Cl^- ions. The chains are along the \hat{b} axis and the planes are in the $(\hat{b}\hat{c})$ plane. (b) Triangular magnetic lattice with exchange couplings of $J_1 = 0.374 \text{ meV}$ and $J_2 = 0.128 \text{ meV}$.

of 3.59 \AA , are situated between the planes and closer to a side of the Cu triangles [13].

The material is an insulator with each magnetic Cu^{2+} ion carrying spin $S = 1/2$. The superexchange routes are mediated by 2 nonmagnetic Cl^- ions and form a frustrated triangular lattice in the $(\hat{b}\hat{c})$ plane, see Fig. 1(b). The anisotropic coupling exchange constants are $J_1 = 0.374 \text{ meV}$ along the chains (\hat{b} axis) and $J_2 = 0.128 \text{ meV}$ between the chains (\hat{c} axis) [14]. There is a small interplane coupling $J_3 = 0.017 \text{ meV}$ along the \hat{a} direction that leads to long range order below $T_N = 0.62 \text{ K}$ in zero applied field [2]. The order is in the form of a spiral because of the frustrated in-plane couplings [2]. Finally, the strength of the Dzyaloshinskii-Moriya term between the chains is found to be $D_a = 0.020(2) \text{ meV}$ [15]. Because of the frustrated spin geometry on a triangular lattice, a very rich low temperature phase diagram is observed [16, 17].

We have used a solution-growth single crystal of Cs_2CuCl_4 (cut to $3.2 \times 6 \times 1.9 \text{ mm}$). The measurements were done at the National High Magnetic Field Laboratory (NHMFL) in Tallahassee, Florida, using a high homogeneity 15 T sweepable NMR magnet. The temperature control was provided by ^4He variable temperature insert. The NMR data were recorded using a state-of-the-art homemade NMR spectrometer. NMR spectra were obtained, at each value of the applied field, from the sum of spin-echo Fourier transforms recorded at each 50 (or 100) KHz intervals. The shift was obtained from the first spectral moment using a gyromagnetic ratio of the bare ^{133}Cs nucleus, 5.5844 MHz/T .

3. ^{133}Cs Shift Measurements

The ^{133}Cs nuclear spin is $I = 7/2$ and since two Cs sites are both in noncubic environments [18, 19, 20] quadrupolar effects are relevant. Therefore, seven distinct NMR satellite lines are observed for each Cs site, as shown in Fig. 2(a). To the first order, the NMR spectrum consist of the following frequencies [21]

$$\begin{aligned} \omega_{\text{NMR}} = & \gamma(1 + K)H_0 + \\ & \omega_Q(m - 1/2)(3 \cos^2 \theta - 1 + \eta \sin^2 \theta \cos 2\phi), \end{aligned} \quad (1)$$

where γ is the nuclear gyromagnetic ratio of ^{133}Cs , and K is the net shift along the applied field direction and is unique for each site. The second term accounts for the quadrupole interaction, i.e., seven peaks displayed in Fig. 2(a), for each $m \leftrightarrow m \pm 1$ transition. Here, $\nu_Q = 2\pi\omega_Q = 3e^2qQ/(h2I(I - 1))$, Q is the nuclear quadrupole moment, η the asymmetry parameter, and θ and ϕ are the spherical angles between the applied field and the principal axis of the electric field gradient (EFG). The EFG tensors are nearly symmetric for both sites, but their principal axes do not coincide. The quadrupole frequencies were deduced from the quadrupole splitting and are consistent with previously reported high temperature values [18, 19, 20]. We find that:

$$\begin{aligned} (\omega_Q)_a^{\text{CsA}} &= 27(2) \text{ kHz}, & (\omega_Q)_a^{\text{CsB}} &= 8.5(5) \text{ kHz}, \\ (\omega_Q)_b^{\text{CsA}} &= 16(1) \text{ kHz}, & (\omega_Q)_b^{\text{CsB}} &= 6.6(2) \text{ kHz}. \end{aligned}$$

In our samples, these values are temperature and field-independent. Nonetheless, below $T \sim 20$ K, quadrupolar satellites cannot be discerned due to the magnetic line broadening (see Fig. 2(b)). Therefore, at low temperatures the quadrupole frequencies were deduced from the beats in the spin-spin relaxation time profile (see Sec. 5).

The net anisotropic shift consists of several contributions given by

$$K_\alpha(T) = K_\alpha^{\text{orbit}} + K_\alpha^{\text{quad}} + K_\alpha^{\text{hf}}(T), \quad (2)$$

where α refers to the direction of the applied field with respect to crystalline axis. K_α^{orbit} is the orbital shift and is temperature-independent and K_α^{quad} is the contribution from the quadrupole interaction. $K_\alpha^{\text{hf}}(T)$ is the hyperfine shift and is given by:

$$K_\alpha^{\text{hf}}(T) = \mu_B \sum_i g_i A_{\alpha i} \langle S_i \rangle / H_0, \quad (3)$$

where μ_B is the Bohr magneton, $i = \{a, b, c\}$, g_i the anisotropic g-factor, $A_{\alpha i}$ the anisotropic hyperfine tensor, and $\langle S_i \rangle$ is the local spin density of Cu spin in the i direction.

The magnitude of each contribution to the shift is determined. The temperature dependence of the net shift of Cs(A) and Cs(B) sites at $H_0 = 5$ T is shown in Fig. 3. Furthermore, the net shift of Cs(A) site at $H_0 \parallel \hat{b} = 14.6$ T is displayed. It is evident that within the error bars the shift is field independent. Although all the curves display a similar temperature dependence, we note a net difference between the shift of Cs(A) and

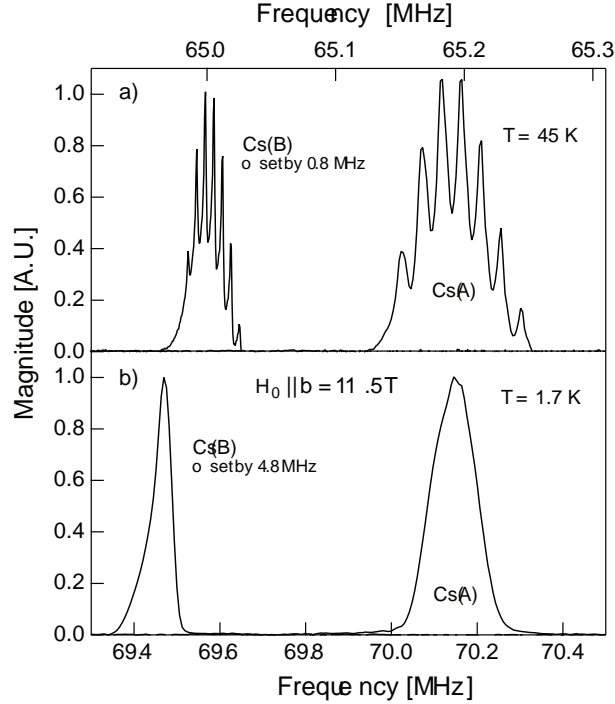


Figure 2. ^{133}Cs NMR resonance frequencies at $T = 45\text{ K}$ (a) and $T = 1.7\text{ K}$ (b) at $H_0 \parallel b = 11.5\text{ T}$. The quadrupole splitting disappears at low temperatures due to magnetic broadening of spectra.

that of Cs(B). At low temperatures, this difference depends strongly on the direction of the field. For a field applied along the crystalline \hat{b} axis, $K_b^{Cs(A)}$ equals approximately $8K_b^{Cs(B)}$, whereas $K_a^{Cs(A)} \sim 4K_a^{Cs(B)}$ for field applied along the \hat{a} axis. This difference cannot be accounted for by a dipole-dipole interaction since the position of Cs(A) and Cs(B) are approximately the same with respect to the Cu atom. Indeed, calculations of the dipolar fields confirm this supposition. Therefore, the difference is caused, most likely, by a strong anisotropic transferred hyperfine interaction with the Cu spins via the Cl atoms.

The temperature dependence of the shift can be expressed in the following form,

$$K(T) = K^{orbit} + \frac{C}{T - \theta_{cw}}, \quad (4)$$

where K^{orbit} is the temperature independent orbital shift, C a constant, and θ_{cw} is the Curie-Weiss temperature. High-temperature series expansion [22] implies that $\theta_{cw} = -(J_2 + J_1/2)$, which equals 3.63 K for Cs_2CuCl_4 . This value of θ_{cw} provides a good fit for the temperature dependence of the data for $T \gtrsim 8\text{ K}$ as illustrated in Fig. 3. If we allow θ_{cw} to be a free fitting parameter, we obtain small positive values for the Curie-Weiss temperature for shift data for both Cs sites and all values of the applied magnetic field. The result is in agreement with the predictions of high-temperature series expansion calculation. This demonstrates that the fluctuations are antiferromagnetic-like for temperatures higher than $\sim 8\text{ K}$ at all values of the applied field. Deviations

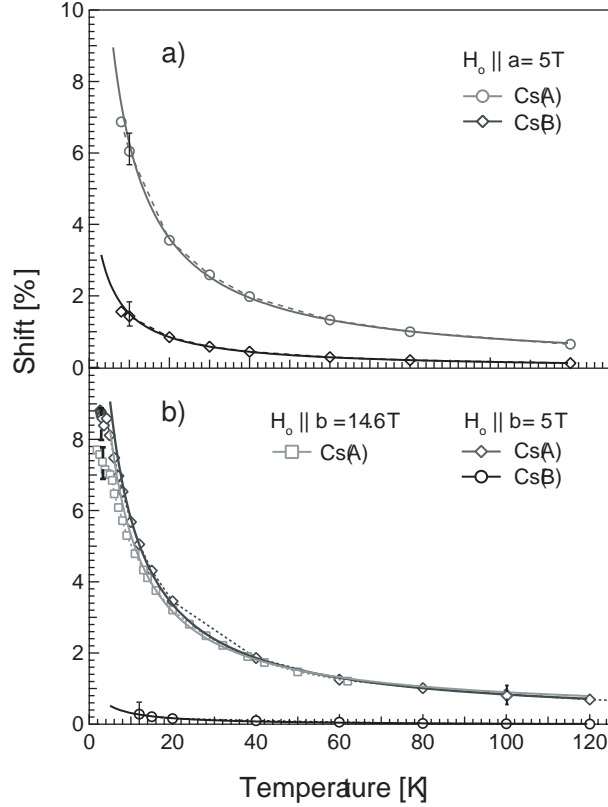


Figure 3. Net shift as a function of temperature at $H_0 = 5$ T field applied parallel to \hat{a} axis, **(a)**, and parallel to \hat{b} axis, **(b)**. The dashed lines are guide to the eye. Typical error bars are shown. The solid lines are fit to Eq. (4). The net shift is nearly isotropic for Cs(A), but highly anisotropic for Cs(B), its value for $H_0 || \hat{a}$ being more than twice the value for $H_0 || \hat{b}$.

from the Curie-Weiss temperature dependence are observed below $T \sim 8$ K. This is indeed expected as a precursor of a short range order phase that develops in the vicinity of $T \sim 2.5$ K for all direction of the applied field [16].

In Fig. 4 the Clogston-Jaccarino plots [23], used to determine hyperfine coupling constants and orbital shifts, are shown. More precisely, the slope of the graph is related to the strength of the hyperfine coupling, while the zero intercept gives the orbital shift. Bulk susceptibility data can be fit to the anisotropic Curie-Weiss law $\chi = C/(T - \theta)$ with $C = N_A g^2 \mu_B^2 S(S + 1)/3k_B$ giving $\theta = 4.0 \pm 0.2$ K, for $T > 20$ K, and g-factors of $g_a = 2.27$, $g_b = 2.11$, $g_c = 2.36$ along the \hat{a} , \hat{b} and \hat{c} axes, respectively [16]. Linear behavior, of the form $K_\alpha = K_\alpha^{orb} + m_\alpha \chi$, is found for $T > 8$ K. Assuming that K_α^{hf} equals to $g_\alpha A_{\alpha\alpha} \chi$, we infer $A_{\alpha\alpha} = m_\alpha/g_\alpha$ in the units of $[T/\mu_B]$:

$$A_a^{Cs(A)} = 0.83(2) \text{ T}/\mu_B, \quad A_b^{Cs(A)} = 0.96(2) \text{ T}/\mu_B,$$

$$A_a^{Cs(B)} = 0.20(2) \text{ T}/\mu_B, \quad A_b^{Cs(B)} = 0.06(1) \text{ T}/\mu_B.$$

The results are obtained at $H_0 = 5$ T. Moreover, the measurements at $H_0 = 5$ T give $K_\alpha^{orbit} = -0.03(5)\%$, but measurements at higher field ($H_0 > 12$ T) give

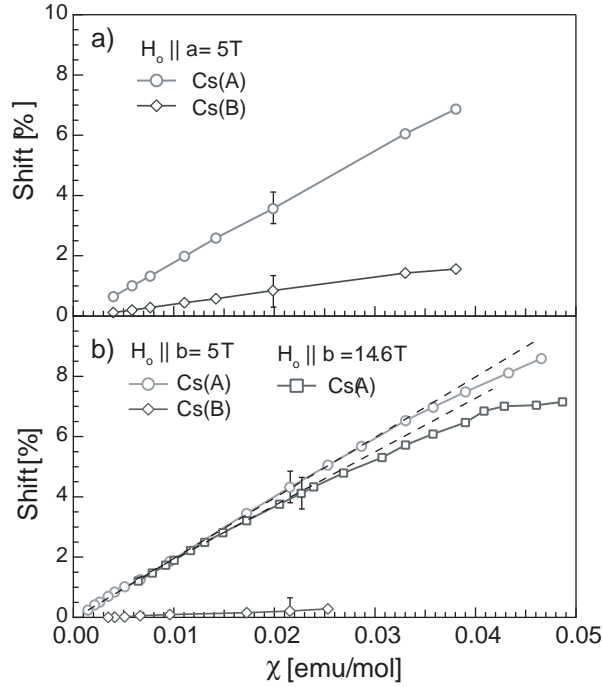


Figure 4. ^{133}Cs Clogston-Jaccarino plots at $H_0 = 5 \text{ T}$. **(a)** For field applied along \hat{a} . **(b)** For field applied along \hat{b} . Black dashed lines are linear fits to the data.

$K_\alpha^{\text{orbit}} = 0.3(1)\%$. In either case, the orbital shift is negligible compared to the dominant magnetic shift at low temperatures.

From these results, we note that the hyperfine coupling is stronger at Cs(A) than at Cs(B). What is more, a more pronounced anisotropy is seen at Cs(B): the hyperfine coupling is more than three times stronger for a field applied along the \hat{a} direction than when H_0 is parallel to \hat{b} . The anisotropy for Cs(A) site is weak.

The values of the hyperfine coupling constants are in agreement with the internal field measured at full polarization. Since at low temperature all the spins are polarized along the applied field for $H_0 > H_{\text{sat}}$, we can assume that $H_\alpha^{\text{int}} = \mu_\alpha A_{\alpha,\alpha}$. By taking the magnetic moment at full polarization to be $\mu = (1.104 \mu_B, 1.04 \mu_B, 1.17 \mu_B)$ [14, 16], and the H^{int} values as described in [24] and Sec. 6, we obtain:

$$\begin{aligned} A_a^{\text{Cs(A)}} &= 1.02 \text{ T}/\mu_B, & A_a^{\text{Cs(B)}} &= 0.25 \text{ T}/\mu_B, \\ A_b^{\text{Cs(A)}} &= 1.11 \text{ T}/\mu_B, & A_b^{\text{Cs(B)}} &= 0.09 \text{ T}/\mu_B, \\ A_c^{\text{Cs(A)}} &= 1.24 \text{ T}/\mu_B, & A_c^{\text{Cs(B)}} &= 0.074 \text{ T}/\mu_B. \end{aligned}$$

These values are somewhat higher than the values found using the shift measurements, but the ratios are the same. We emphasize that these values remain, to a good approximation, independent of the applied field and temperature.

The small quadrupole interaction of the order of tenths of kHz leads to a negligible quadrupolar shift of the order of $\sim \omega_Q^2/\omega_0$, i.e. 0.05 % of the magnetic hyperfine shift. Moreover, since the orbital shifts are small, the major contribution to the shift comes from the hyperfine interaction between the Cs and Cu spins. Therefore, NMR on ^{133}Cs

is a good probe of magnetic degrees of freedom, and the local spin density is accessible via the measurement of the hyperfine fields, see Eq. (3).

We were unable to detect the Cu NMR signal due to fast electronic spin fluctuations that lead to very fast nuclear spin relaxation times of the order of $\hbar/J \sim 10^{-13}$ s. However, the chlorine signal was detected at low temperatures at applied fields stronger than 12 T. It is evident that the Cl nuclear spins, situated along the exchange path, sense strong electronic spin fluctuations. This leads to an extremely fast spin-spin relaxation rate that inhibits detection of the signal. As the field increases, the fluctuations are damped due to the opening of the spin gap. Consequently, the relaxation rate is slowed down and the signal becomes detectable. An average internal hyperfine field sensed by the Cl is $H_{hf} \sim 4.6$ T. This is large compared to internal field ($H_{hf} \sim 1$ T) sensed by the Cs(A).

4. Spin-Lattice Relaxation Time and the Spin Gap

At low temperature ($T = 0.2$ K), a fully spin-polarized state is achieved when the applied field exceeds the saturation field, $H_{sat} \simeq 8.44$ T along \hat{a} and $H_{sat} \simeq 8.5$ T along \hat{b} [15, 16]. In this regime, the ground state is ferromagnetic and excitations are gapped magnons with a gap value that increases with the increasing field. The field dependence of the gap is given by

$$\Delta_H = g\mu_B(H_0 - H_{sat}), \quad \text{for } H_0 > H_{sat}, \quad (5)$$

and $E_{sat} \equiv g\mu_B H_{sat}$. This state has been extensively studied by neutron scattering [15]. The spin-lattice relaxation rate (T_1^{-1}) measurements provide an alternative method to probe this ferromagnetic region, potentially confirm the results obtained by neutron experiments, and thus demonstrate that ^{133}Cs NMR is a good probe of magnetism in Cs_2CuCl_4 .

At high temperatures T_1^{-1} is dominated by phonon contributions [20, 21]. Crucial measurements for determining the value of the spin gap are performed at lower temperatures, where spectra are very broad and quadrupolar satellites cannot be discerned (see Fig. 2). Low temperature spectra are broader than the excitation width of a typical RF pulse. Therefore, to be able to saturate nuclear spin magnetization

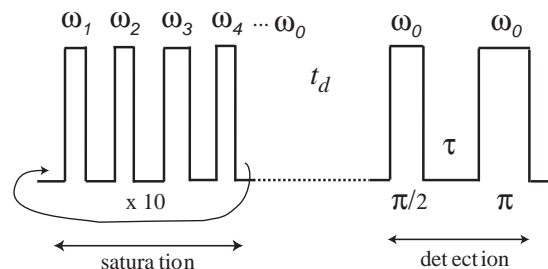


Figure 5. Sketch of a typical pulse sequence used to measure T_1^{-1} rate.

we had to sweep the frequency of the excitation pulses across the line. More precisely, the magnetization was saturated by applying a train of $\frac{\pi}{2}$ pulses equally spaced by a time $t < T_2$ at different frequencies across the line, as illustrated in Fig. 5. The length of pulses was varied depending on their frequency, in order to correctly account for the variation of $\frac{\pi}{2}$ pulse lengths for different satellite transitions [21]. Repeating this sequence for at least 10 times ensured a complete saturation of the nuclear magnetization. Following the saturation pulse train, the signal was detected after a variable delay time τ using a standard spin echo sequence. The length of the detection pulses was tuned so that only a signal from a narrow region around the peak of the spectra, *i.e.*, around the central ($+1/2 \leftrightarrow -1/2$) transition, was detected. This procedure assured that the magnetization relaxation curves are simple exponential functions of time.

In Fig. 6(a) the temperature dependence of T_1^{-1} of Cs(A) is shown at 12 T and 14.6 T fields applied along the \hat{b} axis. The rate approaches a constant in the paramagnetic limit ($T \sim 50$ K) and decreases exponentially at low temperature. The low temperature behavior of T_1^{-1} is an indication of the opening of a gap to spin-flip excitations above the ferromagnetically aligned ground state. The spin-lattice relaxation process requires an energy transfer of $\hbar\omega_{\text{NMR}}$ of the order of 1 mK on the temperature scale. This is negligible compared to the spin gap (*i.e.*, the minimum energy to create a magnon) $\Delta_{\text{H}}/k_B \sim 1$ K. Thus, the relaxation is only effective through the creation of two or more magnons in predominantly one channel [25, 26] in the relevant field range. More precisely, intrabranched transitions involving two magnons with the same S_z dominate the low temperature relaxation process. These have energy close to Δ_{H} and imply that the temperature dependence of the spin-lattice relaxation rate is given by [27]:

$$T_1^{-1} \propto \exp(-\Delta_{\text{H}}/k_B T), \quad (6)$$

where Δ_{H} is defined in Eq. (5).

Fits to this functional form are displayed as the solid lines in Fig. 6(a). Setting the g factor value to $g_b = 2.103(3)$, as determined by the ESR measurements [28] at $T = 77$ K, we find H_{sat} . The findings are summarized in Table 1(a). In Fig. 6(b) the

Table 1. Experimental value of the g -factor, the saturation field, H_{sat} , and the saturation field energy, E_{sat} , at different applied field (a) and temperature (b).

(a)	11.5 T	12 T	14.6 T
H_{sat}^b [T]	8.0(1)	8.2(1)	8.7(4)
(b)	1.9 K	2.5 K	12 K
g_b	2.19(4)	2.13(7)	2.3(2)
$(g_b)_{\text{mean}}$	2.16(6)		-
H_{sat}^b [T]	8.2(1)		8.7(1)
E_{sat} [meV]	1.04	1.01	1.16

rate data is displayed on a log-inverse plot. The low temperature slope is given by $-g_b\mu_B(H_0 - H_{\text{sat}})$. This graph shows that up to $T \sim 5$ K, $\ln(T_1^{-1})$ is indeed a linear function of T^{-1} .

Assuming that the saturation field is approximately 8.5 T for $H_0 \parallel \hat{b}$, one finds that $\Delta_H/k_B = g\mu_B(H_0 - H_{\text{sat}})/k_B$ ranges from 4 K to 8 K in the applied field range. This implies that at low temperatures, $T \lesssim 5$ K, the 2-magnon intrabranh process (involving energies of the order of ~ 6 K) is favored compared to the other intrabranh processes, such as 3-magnon ones sensitive to the energies of the order of $2\Delta_H/k_B \sim 12$ K.

In Fig. 6(c) T_1^{-1} as a function of the applied field parallel to \hat{b} axis at different temperatures is displayed. A fit to Eq. (6) provides a way to independently deduce both

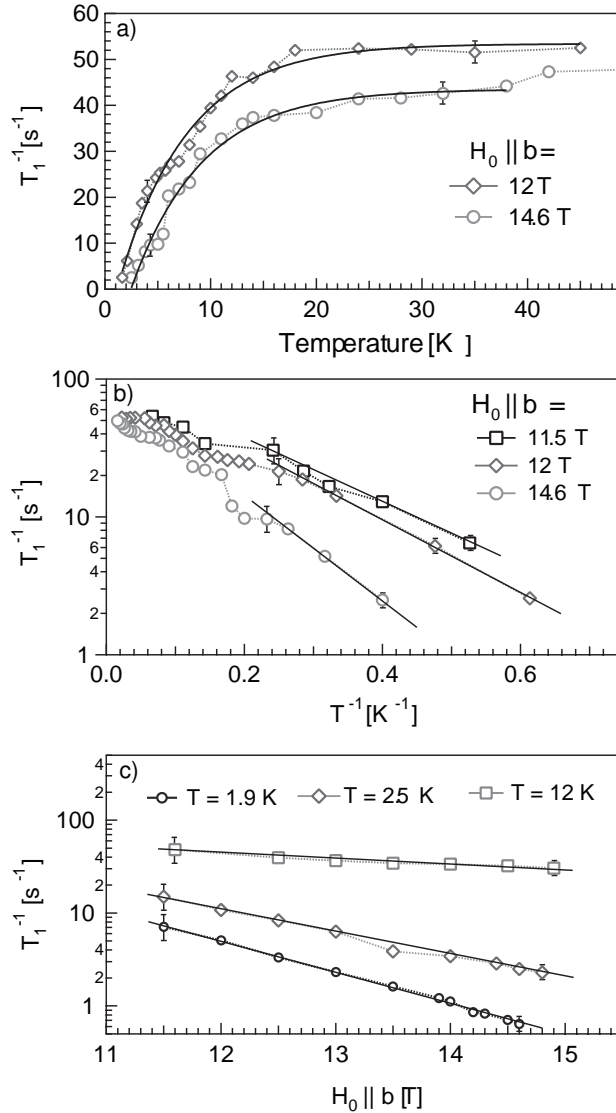


Figure 6. (a) T_1^{-1} rate measurement as a function of temperature for different values of the applied field, $H_0 \parallel b$. (b) A log-inverse plot of (a) showing linear behavior at low temperatures. (c) T_1^{-1} as a function of the field at different temperatures. The solid lines are fit to functional forms described in the text.

H_{sat} and g values for the data. The results are presented in Table 1(b). From the low temperature data, $T = 1.9$ K and 2.5 K, we find that $g_b = 2.16(6)$ and $H_{\text{sat}} = 8.2(1)$ T. The value of the saturation field is consistent with the result of the magnetization measurements [16]. At $T = 12$ K, a higher value of $H_{\text{sat}} = 8.7$ T is found. This is to be expected since at $T = 12$ K, $k_B T \sim E_{\text{sat}} = g\mu_B H_{\text{sat}}$ and the other, mostly thermal, processes contribute to the rate as well. A relatively small discrepancy between H_{sat} values obtained from 12 K and 2 K data indicates that the 2-magnon intrabranh processes still play a significant role in the relaxation process at 12 K.

A saturation field energy of $E_{\text{sat}} = g\mu_B H_{\text{sat}} = 1.02(2)$ meV is obtained for the low temperature data. The theoretical value of the saturation field energy is given by [15],

$$E_{\text{sat}} = 2(J_1 + J_2) + \frac{J_2^2}{2J_1}, \quad (7)$$

and is equal to $E_{\text{sat}} = 1.021$ meV for Cs_2CuCl_4 with $J_1 = 0.374$ meV and $J_2 = 0.128$ meV. Our result is in agreement with the theoretical prediction. For a field applied along the \hat{a} axis, the neutron experiments [15, 29] report a value of 1.065 meV, consistent with our finding.

5. Spin-Spin Relaxation Time

The quadrupole interaction depends on the crystal structure of the material via the electric field gradient $V_{\alpha\alpha}$. Thus, any variations in the quadrupole splitting is a possible indicator of structural change. However, at low temperature the magnetic broadening of the resonance peak masks the quadrupolar splitting, as shown in Fig. 2b. To assure that no structural change take place in the temperature regime of interest, an alternative method to measure quadrupolar parameters is required. Measurement of the spin-spin relaxation rate, T_2^{-1} , can be employed to infer these parameters [30].

T_2^{-1} is acquired by applying a succession of $\frac{\pi}{2}$ - τ - π - τ -echo pulses with a range of values of the delay time τ . By integrating the spin-echo as a function of the delay time, we have obtained a succession of decreasing beats. In Fig. 7(a), result of a typical T_2 measurement is shown. The relaxation profiles can be fit to an expression given by [30]

$$M(t) = y_0 + Ae^{-(2\tau/T_2)} \cos(\omega_B \tau + \phi). \quad (8)$$

where $M(t)$ is the integrated signal magnitude, ω_B the frequency of the beats, A the amplitude, and ϕ is the phase. A net difference in the frequency of the beats for the two sites is evident in Fig. 7(a) and 7(b). In the case of Cs(B), the frequency is $\omega_B \sim 6.9(2)$ kHz, which is more than double the value $\omega_B \sim 16.2(5)$ KHz found for Cs(A). This suggests that the beats are caused by the quadrupole interaction [30] and that the frequency ω_B simply equals the quadrupole splitting frequency ω_Q . The quadrupolar splitting frequencies inferred from the beats in the T_2^{-1} relaxation profile equal, within error, the ω_Q measured directly from the satellite splitting at high temperatures (see Section III). More importantly, we find the same beat values in all fields and at all temperatures down to 2 K. Fig. 7(c) shows results for Cs(A) at $T = 3.5$ K

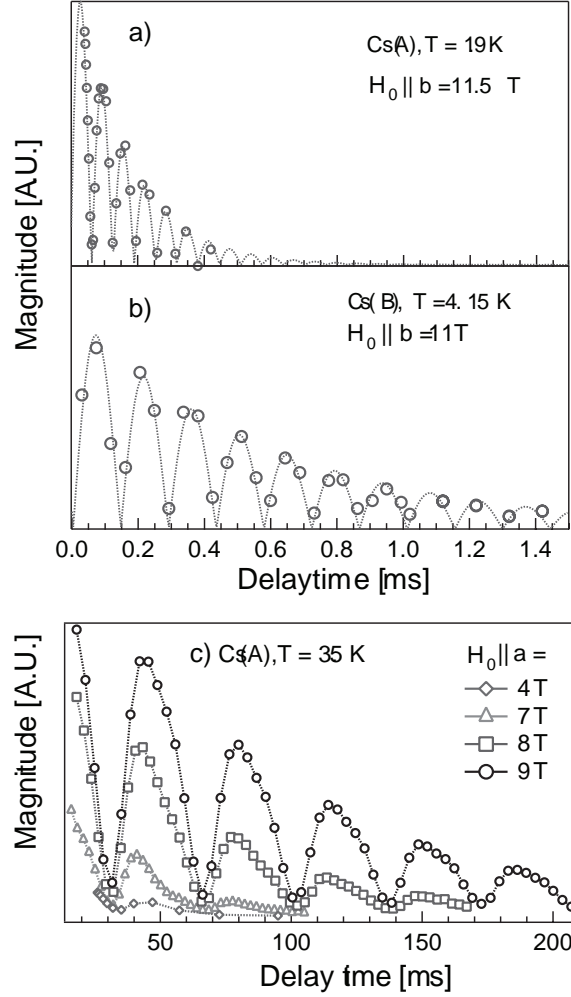


Figure 7. Spin echo amplitude as a function of τ , the delay time, for site Cs(A), (a), and Cs(B), (b). The solid lines are fit to Eq. (8). (c) Spin echo amplitude as a function of the applied field $H_0 \parallel a$ at $T = 3.5$ K for Cs(A), showing no change of the beat frequency as H_0 is varied.

for different fields applied along the \hat{a} axis. We clearly see that the frequency of the beats is unchanged as the applied field is increased. Therefore, we conclude that no significant changes in the crystal structure of the material take place in the temperature and field regime investigated in this work. Finally, the data displayed in Fig. 7(c) indicate that the relaxation time T_2 increases as the field is increased. This is expected since a stronger field freezes the magnetic fluctuations, and therefore slows down the processes that cause spin decoherence.

6. Conclusion

An extensive ^{133}Cs NMR study performed on the 2D frustrated Heisenberg antiferromagnet Cs_2CuCl_4 at temperatures down to 2 K and in a magnetic field up to 15 T, is reported. Spectra are characterised by two main resonance peaks from two

inequivalent cesium sites, referred to as Cs(A) and Cs(B). The net shifts have been deduced for a wide range of fields and temperatures. From these results, we have concluded that the local field is due to a strong transfer hyperfine interaction between the Cu spins and the Cs nuclei. The hyperfine coupling constants have been deduced. They are strongly anisotropic for the Cs(B) site. From the spin-lattice relaxation rate measurements in fields higher than the saturation field, we inferred the values of the g -factor and the saturation field H_{sat} along the \hat{b} axis. These are in agreement with the neutron scattering and magnetization measurement results. Spin-spin relaxation rate measurements are used to deduce quadrupolar splitting frequencies and thus assure that no structural phase transitions take place at temperatures as low as 1.9 K and in magnetic fields up to 15 T.

Our work demonstrates that ^{133}Cs NMR is a good probe of the Cu spin degrees of freedom. The measurements are necessary precursory work to an investigation of the intriguing low temperature magnetic phases. In these phases previous neutron scattering [3] and magnetization measurements [16] have shown evidence for correlated quantum fluctuations enhanced by the low spin and frustrated triangular geometry.

Acknowledgments

We are very grateful to J. B. Marston and S. Ma for helpful discussions. The work was supported in part by the the National Science Foundation (DMR-0547938) and the funds from the Brown University and Salomon Research Fund. The work at the National High Magnetic Field Laboratory was supported by the National Science Foundation under Cooperative Agreement No. DMR95-27035 and the State of Florida.

References

- [1] C. Lhuillier and G. Misguich, "Frustrated Quantum Magnets" in *High Magnetic fields, Applications in Condensed Matter Physics and Spectroscopy*, p. , 161 edited by C. Berthier, L. P. Lévy, and G. Martinez, Springer-Verlag, Berlin (2002); and *cond-mat* 0310405 (2003).
- [2] R. Coldea, D. A. Tennant, A. M. Tsvelik, and Z. Tylczynski, Phys. Rev. Lett. **86**, 1335 (2001).
- [3] R. Coldea, D. A. Tennant, and Z. Tylczynski, Phys. Rev. B **68**, 134424 (2003).
- [4] C.H. Chung, K. Voelker, and Y.B. Kim, Phys. Rev. B **68**, 094412 (2003).
- [5] C. H. Chung, J. B. Marston, and R. H. McKenzie, J. Phys. Condens. Matter **13**, 5159 (2001).
- [6] Yi Zhou and X.G. Wen, *cond-mat* 0210662 (2002).
- [7] S.V. Isakov, T. Senthil, and Y.B. Kim, Phys. Rev. B **72**, 174417 (2005).
- [8] J. Alicea, O. Motrunich, and M. P. A. Fisher, Phys. Rev. Lett. **95**, 247203 (2005).
- [9] S. Yunoki and S. Sorella, *cond-mat* 0602180 (2006).
- [10] M. Y. Veillette, A. J. A. James and F. H. L. Essler, Phys. Rev. B **72**, 134429 (2005).
- [11] D. Dalidovich, R. Sknepnek, A. J. Berlinsky, J. Zhang, and C. Kallin, Phys. Rev. B **73**, 184403 (2006).
- [12] S. Bailleul *et al.*, C. R. Acad. Sci. Ser. 2 **313**, 1149 (1991).
- [13] J.A. McGinney, J. Am. Chem. Soc. **94**, 8406 (1972).
- [14] R. Coldea *et al.*, J. Phys. Condens. Matter **8**, 7473 (1996).
- [15] R. Coldea *et al.*, Phys. Rev. Lett. **88**, 137203 (2002).
- [16] Y. Tokiwa *et al.*, Phys. Rev. B **73**, 134414 (2006).

- [17] M.-A Vachon and V. F. Mitrović, *to be published*.
- [18] H. Hartman, W. Strhlow, H.Z. Haas, Z. Fur. Naturforsch. **A23**, 2029 (1968).
- [19] T. O. Klaassen *et al.*, Physica **64**,149 (1973).
- [20] A.R. Lim, K.S. Hong, and S.-Y. Jeong, J. Phys. Chem. Solids **65**, 1373 (2004).
- [21] A. Abragam, *The principle of Nuclear Magnetism*, Oxford University press (1961).
- [22] Weihong Zheng, Rajiv R. P. Singh, Ross H. McKenzie, and Radu Coldea, Phys. Rev. B **71**, 134422 (2005).
- [23] A.M. Clogston, V. Jaccarino, and Y.Yafet, Phys. Rev. **135**, A650 (1964).
- [24] Precise values of H^{int} was determined from the shift of the NMR line measured at low temperatures ($T < 100$ mK) and high fields ($H_0 > 12$ T).
- [25] D. Beeman and P. Pincus, Phys. Rev. **166**, 359 (1968).
- [26] J. Sagi and I. Affleck, Phys. Rev. B **53**, 9188 (1996).
- [27] M. Troyer, H. Tsunetsugu, and D. Würtz, Phys. Rev. B **50**, 13515 (1994).
- [28] Mark Sharnoff, J. Chem. Phys. **42**, 3383 (1965).
- [29] T. Radu *et al.*, Phys. Rev. Lett. **95**, 127202 (2005); *ibid.* **96**, 189704 (2005).
- [30] H. Abe, H. Yasuoka, and A. Hirai, J. Phys. Soc. Jap. **21**, 77 (1966).